Nuclear Engineering and Design 267 (2014) 164–171

Contents lists available at ScienceDirect

Nuclear Engineering and Design

journal homepage: www.elsevier.com/locate/nucengdes

Unsteady turbulent flow in 90° bend under the wall thinning degradation environment

H.P. Rani [a,*], T. Divya [a], R.R. Sahaya [b], Vivekanand Kain [c], D.K. Barua [b]

[a] Department of Mathematics, NIT Warangal, India
[b] Nuclear Power Corporation of India Limited, NU Bhavan, Anushakti Nagar, Mumbai, India
[c] Material Science Division, Bhabha Atomic Research Center, Mumbai, India

ARTICLE INFO

Article history:
Received 17 July 2013
Received in revised form
18 November 2013
Accepted 21 November 2013

ABSTRACT

A detailed investigation of fully developed transient flow in a 90° bend has been undertaken. The demineralised water has been considered as the working fluid under the operating conditions of wall thinning degradation mechanism in Indian nuclear power plant (NPP). The large eddy simulation (LES) model was employed to compute the large eddies and sub grid scale model was employed to compute the small eddies (unresolved eddies). The LES uses a spatial filtering approach to separate the large and small eddies instead of time averaging operation. The considered flow is of transient nature, hence, apart from the initial disturbances, the flow is observed to be quite random and continuously oscillating with the mean flow for all time. The swirling nature is captured in terms of streamlines at different cross sectional planes. Also the streamlines were captured at a critical sectional plane for every minute. The swirling nature, in terms of large and small eddies, is observed to be strong in the vicinity of the bend. The swirling strength was calculated and it is observed to be more at the bend as well as at the downstream of bend. The flow instability is analyzed and captured in terms of transient iso-surfaces of axial velocity. Also the most important parameter which is vulnerable to flow accelerated corrosion (FAC) i.e., mass transfer coefficient is calculated and analyzed. These results will help to analyze the transient variations in pipe at the locations which are vulnerable to FAC.

1. Introduction

Apart from being of practical importance in connection with various engineering applications, the study of unsteady turbulent pipe flow is of important value in providing the information which can lead to an improved understanding of the phenomenon of turbulence. In such flows certain fundamental aspects of turbulent flow are exposed. Even though these aspects present in steady turbulent flows, they are not apparent under the steady conditions. In addition, due to the effect of inertia, some additional features of turbulence specific to transient flows can be present. Due to the severe technical difficulties involved, detailed measurements of turbulence in transient flow were not possible until quite recently. As a result of the availability of modern instrumentation and powerful computers, transient turbulent flow can now be readily investigated. Accordingly, such flows have begun to receive more extensive study.

Piping system in NPP is usually structured with bends, sudden expansions, sudden contractions and valves. The operation of automatic control systems is all capable of generating high pressure waves in turbulent flow of water through this system. These transient conditions resulting in high pressures can cause pipe failures by damaging the valves and fittings (Kluwick and Stross, 1980; Vasil'ev and Kvon, 1971; Yongmann, 2005). This pipe wall thinning degradation mechanism is known as FAC (Singh et al., 2012; Roychowdhury et al., 2012; Kanster et al., 1990; Vivekanand et al., 2008; Kang and Jo, 2008; Pietralik and Schefski, 2011; Fingjun et al., 2008; Gammal et al., 2012; Kim et al., 2008). The mechanism of FAC is in a sequence process of three steps, i.e., electrochemical oxidation of metal atoms to from ferrous ions at the metal surface, followed by the diffusive mass transfer and then convective mass transfer of ferrous ions in to the bulk water flow. This mechanism is influenced by so many parameters, such as flow parameters, material parameters and water chemistry. Also this over all process is fully time dependent. Hence, the motivation of the present study is to examine the FAC phenomenon in a 90° bend under the transient conditions so as to analyze some of the flow parameters under the conditions of Indian NPP.

To capture the unsteady turbulence the large eddy simulation (LES) model was employed (Versteeg and Malalasekera, 2007; Kawanabe et al., 2007; Sagaut, 1998). Adrian et al. (2000) analyzed and interpreted the instantaneous turbulent velocity fields

* Corresponding author. Tel.: +91 870 246 2834; fax: +91 870 246 2834.
E-mail address: hprani@nitw.ac.in (H.P. Rani).

0029-5493/$ – see front matter © 2013 Elsevier B.V. All rights reserved.
http://dx.doi.org/10.1016/j.nucengdes.2013.11.077

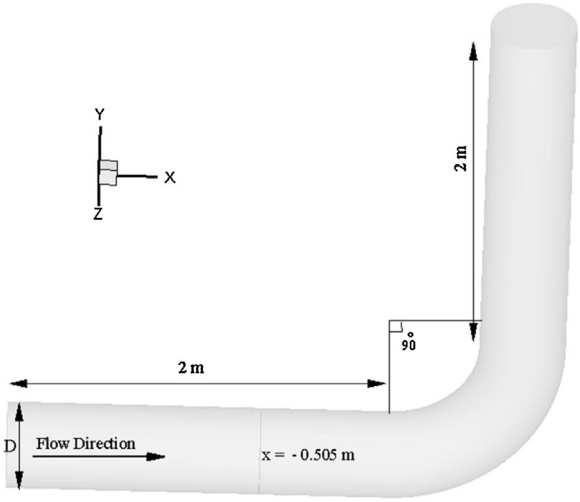

Fig. 1. Computational geometry (D = 0.3405 m).

by using the LES model. LES model was used for many applications of turbulent flow in different geometries such pipe flow (Rudman and Blackburn, 1999) and channel flow (Yang and Ferziger, 1993). The Reynolds averaged Navier–Stokes (RANS) turbulence models are not useful for large extent differences in the behavior of large and small eddies. The universal behavior of small eddies at high Reynolds number can be captured by using the RANS turbulence model, where as it is complicated to capture the large eddies using this model. While the LES model computes the large eddies with a time dependent solution.

The large eddies along with small eddies are clearly captured by this model. Eddies are shown in terms of the streamlines at different cross sectional planes and at different times. The swirling nature and its strength are captured in terms of iso-surfaces. The instability of the flow is studied at different times. Also the most important parameter, that predicts the locations which are susceptible to FAC, is the mass transfer coefficient and is it analyzed at different times.

2. Mathematical formulation

Feeder pipe made of carbon steel material is an integral part of the main boiler feeder pump discharge (MBFPD) and high pressure heater discharge (HPHD) line of feeder piping system. They carry the demineralised water from the reactor fuel channels to remove the heat produced by the fission of uranium fuel. The Indian feeder pipe of 90° bend has been considered for the FAC analysis as shown in Fig. 1. Demineralised water flow is assumed to arrive from a circular inlet channel of diameter (D) 0.34 m. The bend is assumed to be located at 2 m length from downstream of the inlet along x-direction. The physical domain was considered long enough to avoid the significant changes in the flow at the inlet and outlet section of the elbows.

The continuity equation along with the spatially filtered Navier–Stokes equation obtained by large eddy simulation (LES), energy equation and species transport equation have been employed as a mathematical model for a the present problem of transient turbulent flow of an incompressible viscous fluid passing through a 90° pipe. The isotropic behavior of small scale eddies can be captured by the RANS calculations and by improving the mesh resolution. On the other hand, the large eddies, which interact with and extract energy from the mean flow, are more anisotropic and their behavior is dictated by the geometry of the physical domain, the boundary conditions and the body forces. The RANS equations are used to study the overall behavior of all smaller and larger eddies and are described by a single turbulence model. If the problem depends mainly on the large eddies, then it is complicate to select a model from the widely applicable models such as k–ε models and Reynolds stress model. In such cases, a different approach will be adopted to model the large eddies separately with a time dependent simulation. With this knowledge the behavior of small eddies will be modeled quite easier. The LES approach concentrate on these cases (Versteeg and Malalasekera, 2007) is as follows:

2.1. Large eddy simulation (LES) approach

Mathematically, the LES procedure can be thought of as a convolution of the exact turbulent velocity field, $\boldsymbol{u}$ with a filter function $G(\boldsymbol{x}, \boldsymbol{x}', \Delta)$ that gives the resolved scale velocity field $\bar{\boldsymbol{u}}$ as

$$\bar{\boldsymbol{u}}(\boldsymbol{x}, t) = \int\int\int_{-\infty}^{\infty} G(\boldsymbol{x}, \boldsymbol{x}', \Delta)\boldsymbol{u}(\boldsymbol{x}', t)dx'_1 dx'_2 dx'_3 \quad (1)$$

where $\boldsymbol{u} = (u_1, u_2, u_3)$ are velocities in (x_1, x_2, x_3) directions, respectively and over bar indicates the spatially filtering quantities, and $\bar{\boldsymbol{u}}(\boldsymbol{x}, t)$, $\boldsymbol{u}(\boldsymbol{x}, t)$ and Δ are filtered function, original (unfiltered) function and filtered cutoff width, respectively. In three dimensional (3D) computations with grid cells of different length (Δx_1), width (Δx_2) and height (Δx_3), the cutoff width is often taken to be as:

$$\Delta = \sqrt[3]{\Delta x_1 \Delta x_2 \Delta x_3} \quad (2)$$

In common, for most of the selections the above function is same as order of the grid size.

The common forms of the filtering function in the 3D LES computations used for the finite volume implementation is the following Top-hat/box filter function

$$G(\boldsymbol{x}, \boldsymbol{x}', \Delta) = \begin{cases} \dfrac{1}{\Delta^3} & |\boldsymbol{x} - \boldsymbol{x}'| \leq \dfrac{\Delta}{2} \\ 0 & |\boldsymbol{x} - \boldsymbol{x}'| > \dfrac{\Delta}{2} \end{cases} \quad (3)$$

By using the above filtered function, the filtered unsteady Navier–Stokes equations along with the LES continuity equation for an incompressible flow are as follows:

$$\nabla \cdot \bar{\boldsymbol{u}} = 0 \quad (4)$$

$$\frac{d\bar{\boldsymbol{u}}}{dt} + \nabla.(\overline{\boldsymbol{u}\boldsymbol{u}}) = -\frac{\nabla_p}{\rho} + \nu\nabla^2\bar{\boldsymbol{u}} - (\nabla \cdot (\overline{\boldsymbol{u}\boldsymbol{u}}) - \nabla \cdot (\overline{\boldsymbol{u}\boldsymbol{u}})) \quad (5)$$

where ρ is density, ν is the kinematic viscosity.

The last term of Eq. (5), i.e., $(\nabla \cdot (\overline{\boldsymbol{u}\boldsymbol{u}}) - \nabla \cdot (\overline{\boldsymbol{u}\boldsymbol{u}}))$ is caused by the filtering operation and can be considered as a divergence of a set of stresses $\tau_{ij} (= \overline{u_i u_j} - \bar{u}_i \bar{u}_j)$, where i, j = 1–3.i.e.,

$$\nabla \cdot \left(\overline{\boldsymbol{u}\boldsymbol{u}} - \overline{\boldsymbol{u}}\,\overline{\boldsymbol{u}}\right) = \frac{\partial_{\tau ij}}{\partial x_j} \quad (6)$$

In recognition of the fact that a substantial portion of τ_{ij} is attributable to convective momentum transport due to interactions between the unresolved or sub grid scale (SGS) eddies and these stresses are commonly termed as the SGS stresses. The nature of these contributions can be determined with the aid of a decomposition of a flow variable $\varphi(\boldsymbol{x}, t)$ as the sum of (i) the filtered function $\bar{\varphi}(\boldsymbol{x}, t)$ with spatial variations that are larger than the cut-off width and are resolved by the LES computation and (ii) $\varphi'(\boldsymbol{x}, t)$, which contains unresolved spatial variations at a length scale smaller than the filter cut-off width i.e.,

$$\varphi(\boldsymbol{x}, t) = \bar{\varphi}(\boldsymbol{x}, t) + \varphi'(\boldsymbol{x}, t) \quad (7)$$

By using the above decomposition the SGS stresses or τ_{ij} can be written as follows

$$\tau_{\mathrm{ij}} = \overline{u_i u_j} - \bar{u}_i \bar{u}_j = (\overline{\bar{u}_i \bar{u}_j} - \bar{u}_i \bar{u}_j) + \overline{\bar{u}_i u'_j} + \overline{u'_i \bar{u}_j} + \overline{u'_i u'_j} \quad (8)$$

The above Eq. (8) contains three groups of contributions, namely:

Lernard stresses, $L_{ij} = \overline{\bar{u}_i\bar{u}_j} - \bar{u}_i\bar{u}_j$, due to the effects at resolved scale; cross stresses $C_{ij} = \overline{\bar{u}_i u'_j} - \overline{\bar{u}_i}\,\overline{\bar{u}_j}$, due to the interactions between the SGS eddies and the resolved flow, and LES Reynolds stresses, $R_{ij} = \overline{u'_i u'_j}$, due to convective momentum transfer and interactions of SGS eddies and are modeled with a so called SGS turbulence model.

2.2. Smagorlinksy–Lilly SGS model

In this model the local SGS stresses, R_{ij}, are taken to be proportional to the local rate of strain $\overline{S_{ij}}(= 1/2(\partial\bar{u}_i/\partial_{x_j} + \partial\bar{u}_j/\partial x_i))$ of the resolved flow, i.e.,

$$R_{ij} = 2\mu_{SGS}\overline{S_{ij}} + \frac{1}{3}R_{ij}\delta_{ij} \tag{9}$$

Peyret and Krause (2006) noted that in spite of the different nature of the Leonard stresses and cross-stresses, they are lumped together with the LES Reynolds stresses in the current versions of the finite volume method. The whole stress τ_{ij} is modeled as a single entity by means of a single SGS turbulence model as

$$\tau_{ij} = -2\mu_{SGS}\overline{S_{ij}} + \frac{1}{3}\tau_{ij}\cdot\delta_{ij} \tag{10}$$

where $\mu_{SGS}\left(= \Delta^2|\bar{S}|, \quad \bar{S} = \sqrt{2\overline{S_{ij}}\,\overline{S_{ij}}}\right)$ is the SGS viscosity.

Eqs. (4) and (5) were solved along with the following energy equation

$$\nabla(\bar{u}T) = \frac{1}{\rho}\cdot\nabla\cdot(k_{eff}\nabla T) \tag{11}$$

where T denotes the temperature, k_{eff} is given by $k_{th} + C_p(\mu_{SGS}/pr_t)$, with turbulent Prandtl number $Pr_t = 0.85$ and k_{th} and C_p denotes the thermal conductivity and specific heat at constant pressure, respectively.

The conservation equation for the chemical species, which predicts the local mass fraction of species (ferrous ions) takes the following general form.

$$\nabla\cdot(\bar{u}Y) = \frac{\nabla\cdot J}{\rho} \tag{12}$$

where $J = (\rho D + (\mu_{SGS}/Sc_t))\nabla Y$ denotes the mass diffusion flux of species, in which Sc_t, Y and D are the turbulent Schmidt number ($Sc_t = 0.7$), the local mass fraction of the species and the diffusion coefficient for the species, respectively.

3. The computational procedure and the generated mesh

The numerical simulation of the governing equations (4, 5, 11 and 12) was performed by utilizing the commercially available software, namely ANSYS. In the first analysis phase, the geometry of the flow model was constructed using the preprocessor, namely ANSYS Design Modeler. The uniform grids were generated and clustered near the bends. Fixed time (Δt) step of 0.001 has been chosen for the transient simulations. The stability and accuracy of the solution was ensured by maintaining Courant number ($Cu = \bar{\boldsymbol{u}}\Delta t$/cell size) in the range of 0.05–0.02. In each time step 30 number of iterations is employed and they are found to be adequate to achieve the convergence for all time steps. Boundary conditions and other parameter values, under the operating conditions of feeders of Indian NPP are considered and are tabulated in Table 1.

The transitional non-dimensional wall roughness height, $k_s^+(= \rho k_s u^*/\mu)$ is considered to be 2.8, with roughness height k_s (=7.5e^{-5}) (Pietralik and Schefski, 2011). In the above definition u^* represented as $\bar{u}/u^+$ and in the log law layer (as $y^+ < 450$) u^+ is defined as $u^+ = 1/k \ln y^+ + B$ in which κ is the Von-karman's constant (=0.4) and $B = 5.5$ (ANSYS, 2009; Brown, 1997).

Table 1
Indian NPP operating conditions.

Parameter	90° bend
Outside diameter	355.6 mm
Thickness	15.0876 mm
Inner diameter (D)	340.5124 mm
Radius of curvature	510.7686 mm
Material	Carbon steel without chromium content
Fluid	Demineralised water
Temperature	150 °C
Kinematic viscosity (ν)	1.004e−6
Schmidt number (ν/D)	9.2
Reynolds number($\overline{u_1}D/\nu$)	1.016e+6

The PISO (pressure implicit with splitting of operators) algorithm was used along with the staggered grid to simultaneously solve the velocity and pressure equations. The first order upwind scheme was used for discretising convection and diffusion transports on a uniform grid as given in the literature. Second order implicit formulation has been used for the transient calculations. In all the investigations, the iterative calculations of the primitive variables were terminated when the residual norm criteria, 10^{-6} was reached. The convergence of a solution was also checked from the mass flow summary. The computations were carried out using the workstation namely, HP Z800 Intel Xeon Dual Core Processor.

The mesh density has been varied so that the computed solutions represent the real flow physics. A series of grid independence tests was conducted to determine the optimal mesh. The solution obtained through three different number of grid nodes, by considering three different Cu values 0.05, 0.1 and 0.2 for the fixed time step ($\Delta t = 0.001$) value. The solution of these grid systems is compared in terms of pressure contours at a cross section plane $y = 0$ for a fixed time. Fig. 2 shows the comparison of these results and it is observed that for Cu = 0.1 and 0.2 gives the similar results in comparison with that of Cu = 0.05. Hence the grid system of Cu = 0.1 was employed for the present study.

4. Results and discussion

The flow parameters and their structures are analyzed in terms of contours, streamlines and iso-surfaces with respect to time. Since flow is of transient nature, apart from the initial disturbances, the flow is quite random and continuously oscillating with the mean flow for all time. These variables are calculated at critical cross sectional planes where the flow parameters play an important role these results will help to identify the reason that leads to failures in the pipe. Also the mass transfer has been analyzed in terms of mass transfer coefficient (MTC), since this is the most important parameter to predict the locations susceptible to FAC.

4.1. Velocity, pressure and dot product of velocity and helicity

The axial velocity ($\overline{u_1}$ and pressure (p) for showing the fluctuating nature of the flow motion is computed and is shown in Fig. 3. The random nature of the each variable is observed with respect to time at a point (0.3845, −0.335571, 0.001928) m in the critical region i.e., near the bend. Each variable is the combination of steady mean value and a fluctuating value. The turbulent fluctuations always have a 3D spatial character, while mean values vary in only one or two space dimensions. It is observed form the figure that $\overline{u_1}$ and p have the oscillating, non-periodic and random behavior.

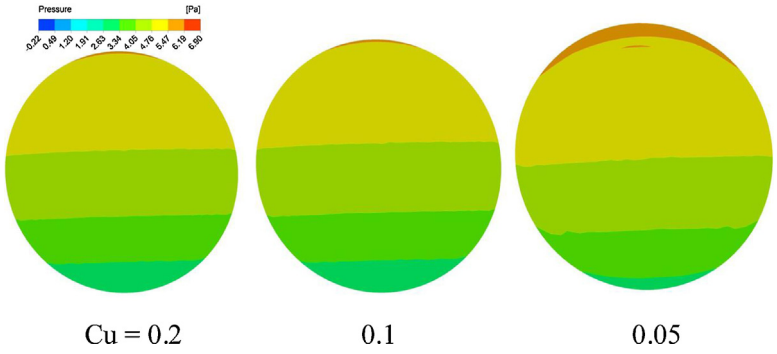

Fig. 2. Grid independence test for different Cu.

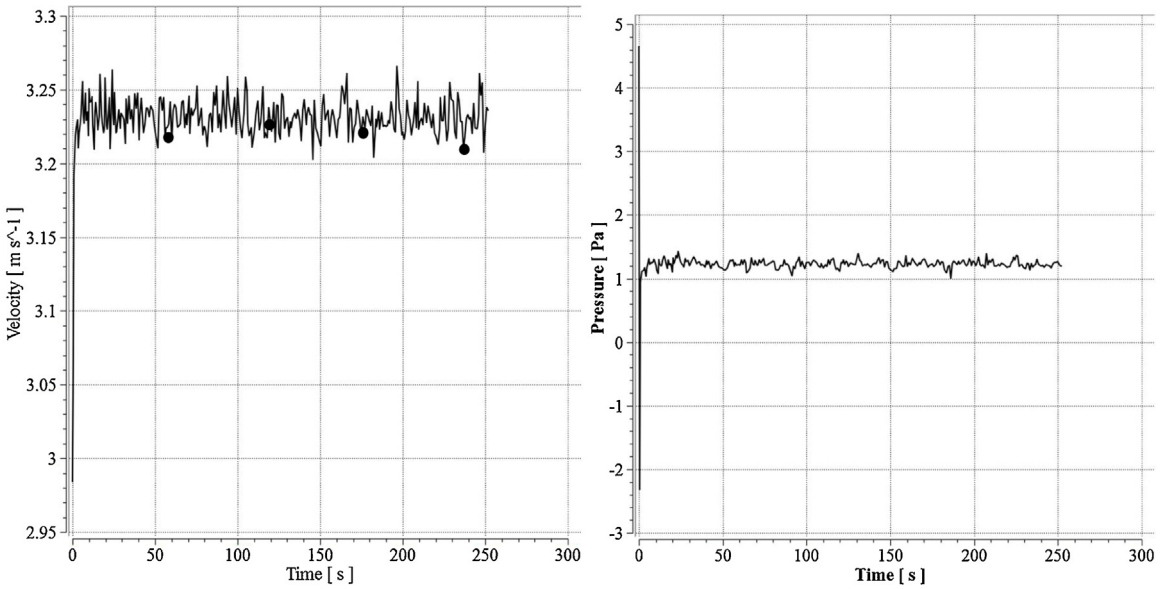

Fig. 3. At the critical point (0.3845, −0.335571, 0.001928) m velocity and pressure. The dot symbols (•) represent the every minute of time at which the instantaneous variables are captured.

4.2. Vortical flow structure

Fig. 4 shows the presence of vortices at different sectional planes such as, at the upstream of bend ($x = -0.505$ m), at the center of bend ($\theta = 45^\circ$) and at the downstream of bend ($y = 0.5054$ m) at $t = 4$ min. From the sectional planes it is observed that large eddies and small eddies are clearly delineated with the help of LES model. The vortices are more in number at the downstream and upstream sectional planes of the bend comparing with that of the vortices in a plane, which is at the middle of the bend. The increasing number of vortices is due to the centrifugal instability at that cross sectional planes. The vortices formed near the wall region are termed as weak vortices and vortices formed at the center of the sectional plane are termed as strong vortices (Tsai and Sheu, 2007). At the upstream sectional plane ($x = -0.505$ m) more number of vortices are observed comparing with the other sectional planes. Then in the sectional plane $\theta = 45^\circ$ the vortices near the end wall are vanished and there remains only the center vortices. Finally in the downstream sectional plane these center vortices get divided and formed two more vortex pairs.

In the above discussion, it can be observed that more number of vortices are seen at the upstream sectional plane as shown in

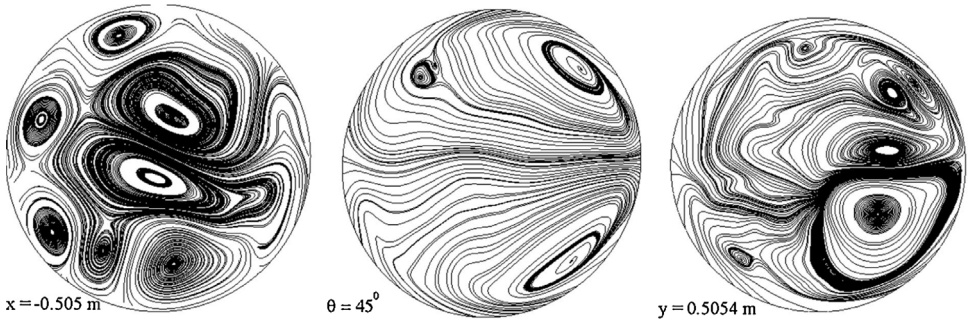

Fig. 4. Streamlines at different cross sectional planes for $t = 4$ min.

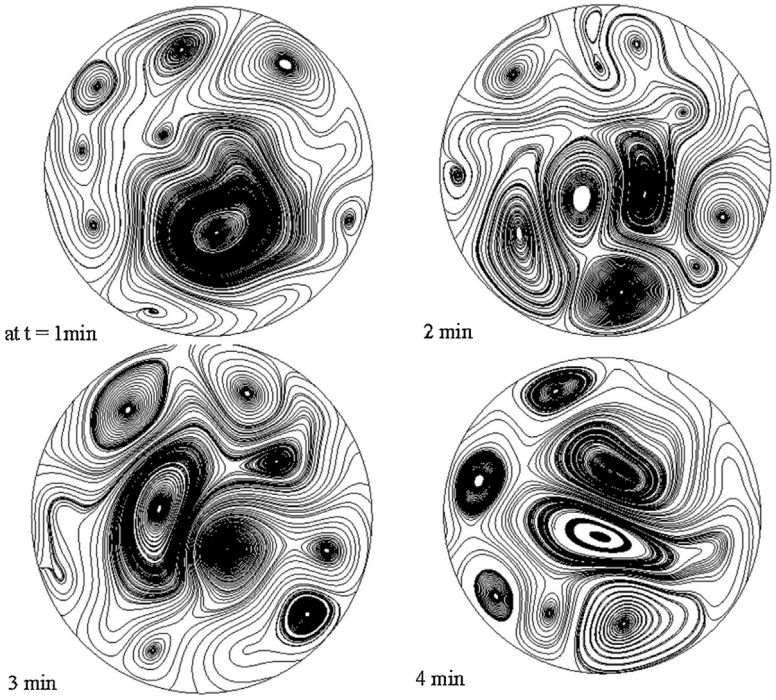

Fig. 5. The instantaneous simulated streamlines at a cross sectional plane $x = -0.505$ m [shown in the Fig. 1].

Fig. 4. Hence the transient turbulence nature is analyzed at this plane ($x = -0.505$ m) and shown in Fig. 5. It is observed from Fig. 5 that the essence of LES model along with SGS model is clearly signified in terms of large and small eddies. As the time varies from $t = 1$ to 2 min the number vortices are increased, and then for $t = 3$ and 4 min the number of vortices are decreased due to the turbulent fluctuations. The variation in number of vortices is proportional to the variation of velocity magnitude with respect to time. It can be seen by intense observation of velocity fluctuations in Fig. 3 for every minute.

The vortex nature shown in Figs. 4 and 5 indicates the existence of swirling flow. To capture the swirling nature, the iso-surfaces of the maximum swirling strength (Img{λ}, where λ is the eigenvalues of tensor τ_{ij}) of 0.727 min^{-1} along with streamlines at the cross sectional plane $z = 0$ are presented in Fig. 6. It is observed that this strength is more at the bend and also at the downstream of the bend. Also the streamlines are swirling around the iso-surface where the swirling strength is high.

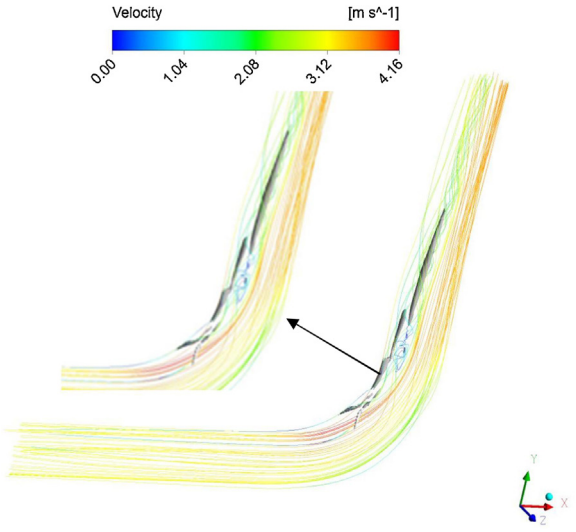

Fig. 6. Iso-surface of the swirling strength (0.727 min^{-1}) of the flow along with the streamlines at the cross sectional plane $z = 0$ at $t = 4$ min.

Instantaneous iso-surfaces of the axial velocity with three different magnitudes such as, positive, negative and zero magnitudes are presented in Fig. 7 for a span of time from $t = 3.97$ to 4.1 min. The positive (accelerated) and negative (decelerated) flows are delineated by the shear layer with zero magnitude axial velocity. Positive magnitude flow leads to the presence of swirling flow and the negative magnitude flow leads to the formation of the recirculation region. In transient flows it is well known from the previous study (Versteeg and Malalasekera, 2007) that the turbulent regimes are susceptible to oscillations. For the incompressible flow the oscillations are caused by the interactions between the shear layer and the re-circulating flow due to the Kelvin–Helmholtz (KH) instability. Due to the KH instability in the shear layer, unsteady vortical structures are generated and convected downstream to produce fluctuations in the velocity and pressure, thus leading to the destabilization of the flow field (Komerath et al., 1987; Freitas and Street, 1988). The strong shear layer is prone to instability which results in the roll-up of the individual co-rotating vortices (Rani et al., 2007). It is observed from Fig. 8 that the behavior is random and unstable with respect to time.

4.3. Mass transfer

The final step of the degradation mechanism i.e., the convective mass transfer step of ferrous ions from the oxide water interface through the boundary layer of water into the bulk of water was analyzed and is given by:

$$F_{fe} = K \cdot (C_w - C_b) \tag{13}$$

where F_{fe} is the mass flux of ferrous ions, K is the mass transfer coefficient (MTC), C_w is the concentration of the ferrous ions at the oxide water interface and C_b is the concentration of the ferrous ions in the bulk fluid. For the long piping the mass transfer analysis is not used directly to calculate FAC rate till the concentration difference of ferrous ions at the oxide water interface and in the

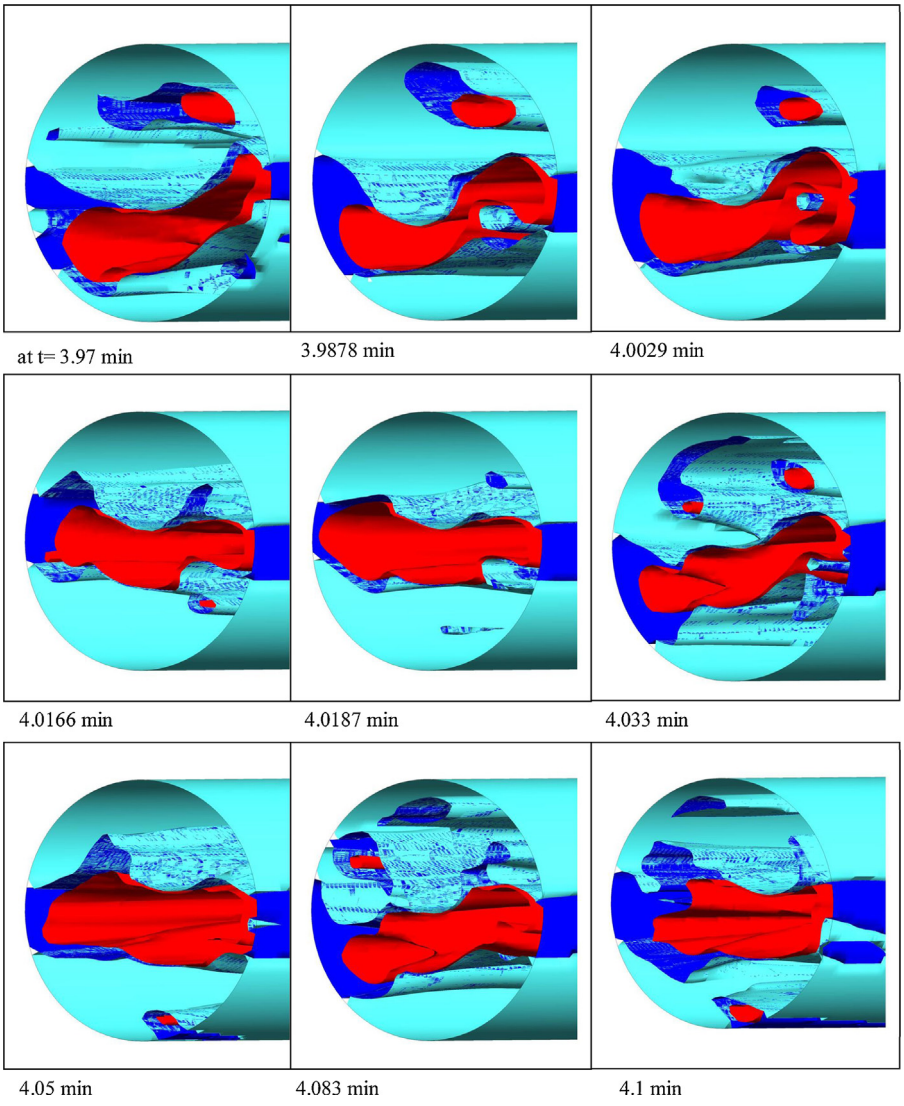

Fig. 7. The instantaneous iso-surfaces of axial velocity. Red, cyan and blue colors denote positive, negative and zero axial velocity values, respectively. (For interpretation of the references to color in this figure legend, the reader is referred to the web version of the article.)

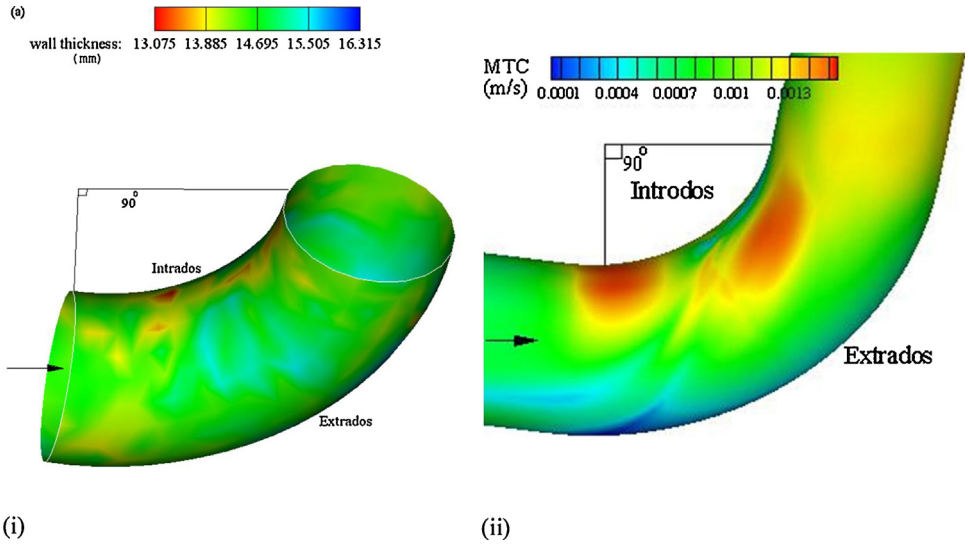

Fig. 8. The contours in a 90° bend under the Indian NPP conditions. (i) measured wall thickness data and (ii) simulated MTC. The arrow indicates the flow direction.

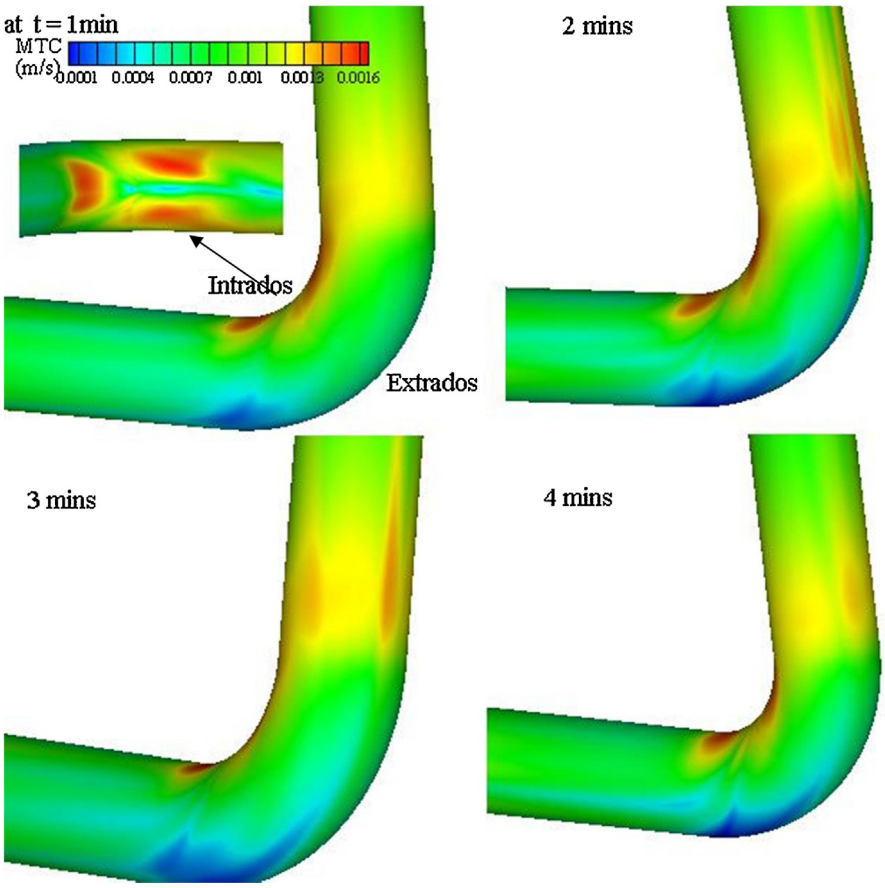

Fig. 9. The instantaneous contours of mass transfer coefficient (MTC).

bulk water (Fingjun et al., 2008; Pietralik and Smith, 2006; Pietralik, 2008) is known. But, the concentration difference depends on the first (oxidation) and second (diffusion) steps of the thinning degradation mechanism. This analysis can be applicable when the piping is short and mass transfer is the dominating factor of the FAC rate. In such cases the FAC rate is converted into the proportionality constant, namely, K (Pietralik and Schefski, 2011). The mass transfer coefficient was analyzed extensively to predict the wall thinning locations under the operating conditions of Indian NPP. Under the turbulent flow conditions the MTC (K) was calculated based on the following Chilton–Colburn equation (Fingjun et al., 2008).

$$K = (\tau_w/\bar{u} \cdot \rho) \cdot Sc^{-2/3} \quad (14)$$

The values of K were calculated based on the simulated results of wall shear stress τ_w (i.e., τ_{ij} at the wall, $i \neq j$).

The comparison of simulated MTC results with that of the wall thinning data of Indian NPP is shown in Fig. 8. The comparison between the two results is found to be in good agreement in terms of locations. It is observed that intrados of the bend is more susceptible to FAC. Also, the instantaneous MTC distribution is calculated using the above correlation given in Eq. (14) and these results are presented in Fig. 9. It is observed that MTC distribution is also varying with respect to time, and the intrados of the elbow is more susceptible to FAC. Initially at $t = 1$ min, the maximum MTC occurs at the intrados of the elbow. As time increases, for $t = 2$ and 3 min, maximum MTC occurs at the extrados also. Thus at $t = 2$ and 3 min extrados of the bend also getting affected along with the intrados. Again at $t = 4$ min at the extrados the MTC value is comparatively less. The oscillation nature of MTC in intrados and extrados is observed for all time.

5. Conclusions

The transient turbulent de-mineralized water flow in a 90° bend pipe has been analyzed under the operating conditions of wall thinning degradation mechanism in Indian nuclear power plant. The spatial filtering approach i.e., large eddy simulation was employed to compute the large eddies and the sub grid scale model to capture the unresolved eddies with respect to time. The vortex nature is captured in terms of streamlines at different cross sectional planes. It is observed that vortices are formed in each cross section and number of vortices is varying for different cross sections. Also observed that the cross sectional plane located at the upstream of the bend have more number of vortices due to instability. The instantaneous behavior of streamlines at the upstream cross sectional plane is observed that, the number of vortices is varying proportionally with respect to the instantaneous velocity magnitude. The formation of eddies and its variations with respect to each sectional plane and time indicates the existence of swirling flow. The swirling flow is analyzed by capturing the iso-surface with maximum swirling strength (0.727 min^{-1}) along with streamlines at the mid plane ($z = 0$). The strength is more at the bend and also at the downstream of the bend due to the presence of strong shear layer. The shear layer prone to instability is captured for a span of time from 3.97 min to 4.1 min by calculating the iso-surfaces of positive, negative and zero axial velocities and observed to have the random behavior. Finally the most important parameter susceptible to FAC i.e., MTC, distribution is calculated with respect to time. It is observed that the intrados of the bend is more susceptible to FAC. From the transient distribution of MTC it is observed that extrados of the bend also slightly getting effected. These results will help to

analyze the transient variations in the pipe at the locations which are vulnerable to FAC.

Acknowledgements

The financial support from the Board of Research in Nuclear Sciences, under BRNS/2009/36/70-BRNS/2390, Department of Atomic Energy is gratefully acknowledged.

References

ANSYS Fluent® version 12.1 Users Guide, 2009.
Adrian, R.J., Christensen, K.T., Liu, Z.C., 2000. Analysis and interpretation of instantaneous turbulent velocity fields. Experiments in Fluids 29, 273–290.
Brown, G.J., 1997. Numerical simulation of separated flows in three-dimensional industrial geometries: a case study, International conference on CFD in Mineral and Metal Processing and Power Generation. CSIRO, 157–164.
Fingjun, L., Lin, Y., Li, X., 2008. Numerical simulation for carbon steel flow-induced corrosion in high-velocity flow seawater. Journal of Anti-Corrosion Methods and Materials 55/2, 66–72.
Freitas, C.J., Street, R.L., 1988. Non-linear transport phenomena in a complex recirculating flow: a numerical investigation. International Journal for Numerical Methods in Fluids 8, 769–802.
Gammal, M.Al., Ahmed, W., Ching, H.C.Y., 2012. Investigation on wall mass transfer characteristics downstream of an orifice. Nuclear Engineering and Design 242, 353–360.
Kang, D.G., Jo, J.C., 2008. CFD application to the regulatory assessment of FAC-caused CANDU feeder pipe wall thinning issue. Journal of Nuclear Engineering and Technology 40 (1), 37–48.
Kanster, W., Erve, M., Henzel, N., Stellwag, B., 1990. Calculation code for erosion corrosion induced wall thinning in piping system. Nuclear Engineering Design 119, 431–438.
Kawanabe, H., Kawasaki, K., Seno, T., Kondo, C., Shioji, M., 2007. LES analysis of flow and turbulent mixing in an unsteady jet. Heat Transfer – Asian Research 36 (5).
Kim, J.W., Na, M.G., Park, C.Y., 2008. Effect of local wall thinning on the collapse behavior of pipe elbows subjected to a combined internal pressure and in-plane bending load. Journal of Nuclear Engineering and Design 238, 1275–1285.
Kluwick, A., Stross, N., 1980. Unsteady, turbulent flow in pipes. Acta Mechanica 37, 1–12.
Komerath, N.M., Ahuja, K.K., Chambers, F.W., 1987. Prediction and measurement of flows over cavities – a survey. AIAA, 87–0166.
Peyret, R., Krause, E., 2006. Advanced turbulent flow computations, CISM Courses and Lectures No. 395. International Centre for Mechanical Sciences, Springer-Verlag, Vienna.
Pietralik, J.M., 2008. Mass transfer effects in feeder flow-accelerated corrosion wall thinning. In: 18th CNS International Conference on CANDU Maintenance, Toronto, Nov. 16–18, CW-33126-CONF-009.
Pietralik, J.M., Schefski, C.S., 2011. Flow and mass transfer in bends under flow-accelerated corrosion wall thinning conditions. Journal of Engineering for Gas Turbines and Power 133, 012902(1–7).
Pietralik, J.M., Smith, B.A.W., 2006. CFD Applications to flow-accelerated corrosion in Feeder Bends. In: Proceedings of the 14th International Conference on Nuclear Engineering (ICONE-14), Miami, FL, July 17–20, p. 89323.
Rani, H.P., Sheu, T.W.H., Tsai, E.S.F., 2007. Eddy structures in a transitional backward-facing step flow. Journal of Fluid Mechanics 588, 43–58.
Roychowdhury, S., Kain, V., Matcheswala, A., Bhandakkar, A., 2012. Sigma phase induced embrittlement in titanium containing austenitic stainless steel tie-bars in a condenser. Engineering Failure Analysis 25, 123–132.
Rudman, M., Blackburn, H.M., 1999. Large eddy simulation of turbulent pipe flow. In: 2nd International Conference on CFD in the Minerals and Process Industries, CSIRO, pp. 503–508.
Sagaut, P., 1998. Large Eddy Simulation for Incompressible Flows. Springer, Germany.
Singh, J.L., Umesh Kumar, Kumawat, N., Sunil Kumar, Vivekanand Kain, Anantharaman, S., Sinha, A.K., 2012. Flow accelerated corrosion of carbon steel feeder pipes from Pressurized Heavy Water Reactors. Journal of Nuclear Materials 429, 226–232.
Tsai, S.F., Sheu, T.W.H., 2007. Numerical exploration of flow topology and vortex stability in a curved duct. International Journal for numerical Methods in Engineering 71, 564–582.
Vasil'ev, O.F., Kvon, V.I., 1971. Unsteady turbulent flow in a pipe. Journal of Applied Mechanics and Technical Physics 12 (6), 899–905.
Versteeg, H.K., Malalasekera, W., 2007. An Introduction to Computational Fluid Dynamics the Finite Volume Method, 2nd ed. Pearson, England.
Vivekanand, K., Roychowdhury, S., Mathew, T., Bhandakkar, A., 2008. Flow accelerated corrosion and its control measures for the secondary circuit pipelines in Indian nuclear power plants. Journal of Nuclear Materials 383, 86–91.
Yang, K.S., Ferziger, J.H., 1993. Large-Eddy simulation of turbulent obstacle flow using a dynamic subgrid-scale model. AIAA 31 (8), 1406–1413.
Yongmann, M.C., 2005. Unsteady turbulent flow with sudden pressure gradient changes. International Journal for Numerical Methods in Fluids 47, 925–930.